

# A simple assembly planner for the insertion of ring-shaped deformable objects

*Ixchel G. Ramirez-Alpizar and Kensuke Harada*

Department of Systems Innovation, Graduate School of Engineering Science, Osaka University, Toyonaka, Japan, and

*Eiichi Yoshida*

CNRS-AIST JRL (Joint Robotics Laboratory), UMI3218/RL, National Institute of Advanced Industrial Science and Technology (AIST), Tsukuba, Japan

## Abstract

**Purpose** – The aim of this work is to develop a simple planner that is able to automatically plan the motion for a dual-arm manipulator that assembles a ring-shaped elastic object into a cylinder. Moreover, it is desirable to keep the amount of deformation as small as possible, because stretching the object can permanently change its size thus failing to perfectly fit in the cylindrical part and generating undesired gaps between the object and the cylinder.

**Design/methodology/approach** – The assembly task is divided in two parts: assembly task planning and assembly step planning. The first one computes key configurations of the robot's end-effectors, and it is based on a simple heuristic method, whereas the latter computes the robot's motion between key configurations using an optimization-based planner that includes a potential-energy-based cost function for minimizing the object's deformation.

**Findings** – The optimization-based planner is shown to be effective for minimizing the deformation of the ring-shaped object. A simple heuristic approach is demonstrated to be valid for inserting deformable objects into a cylinder. Experimental results show that the object can be kept without deformation for the first part of the assembly task, thus reducing the time it is being stretched.

**Originality value** – A simple assembly planner for inserting ring-shaped deformable objects was developed and validated through several experiments. The proposed planner is able to insert ring-shaped objects without using any sensor (visual and/or force) feedback. The only feedback used is the position of the robot's end-effectors, which is usually available for any robot.

**Keywords** Assembly, Motion planning, Deformable object

**Paper type** Research paper

## 1. Introduction

In the past decades, the development and/or improvement of all kind of sensors, vision systems, grippers, etc. has allowed robots to manipulate several types of objects, such as ropes, wires (Wakamatsu *et al.*, 2004) and food products (Friedrich *et al.*, 1996; Sakamoto *et al.*, 2007). This has contributed to the widespread use of industrial robots at factories to automatize manufacturing processes. However, many assembly processes remain a challenging task for robots, because they require mating (fastening) two or more parts. In the particular case of assembly processes involving deformable objects, this can be attributable to the high dexterity needed to manipulate these kinds of objects. In contrast, we (humans) possess (or we are able to get through experience) the dexterity required to handle objects of several types of materials, shapes, sizes, etc. and we also have very fine tactile and vision senses to perform precision and assembly tasks.

In this work, we consider the assembly process of inserting a ring-shaped elastic object into a cylinder as a first step on the

manipulation of deformable objects in assembly tasks. This type of assembly is commonly used in the manufacturing process of machines for sealing pipes against liquids or gases to prevent any leakage. For example, ring-shaped elastic objects commonly known as “o-rings” or packing are frequently used at the automotive industry for the manufacture of engines, fuel systems, air conditioning, transmission, etc., to seal against oil, fuel, air, among others. These o-rings have smaller diameters than the pipes (cylinder) they are used in, thus creating pressure against the pipe and consequently leaving no gap between them and the pipe. Also, they are usually made of materials with relatively high stiffness to endure time, application temperatures and pressure. These inherent features of o-rings have two important implications in assembly tasks. First, large deformations (stress) lead to its deterioration and/or fracture, e. g. the o-ring is not able to return to its original size, thus generating undesired gaps with the pipe, leading to leakage and failures [1]. Second, a considerable amount of force is needed to generate large deformations. Consequently, it is very important to keep the object's deformation as small as possible. For this problem, this paper proposes a simple method that can easily and effectively reduce the amount of elastic deformation during the assembly process.

---

The current issue and full text archive of this journal is available on Emerald Insight at: [www.emeraldinsight.com/0144-5154.htm](http://www.emeraldinsight.com/0144-5154.htm)



Assembly Automation  
38/2 (2018) 182–194  
© Emerald Publishing Limited [ISSN 0144-5154]  
[DOI 10.1108/AA-12-2016-181]

---

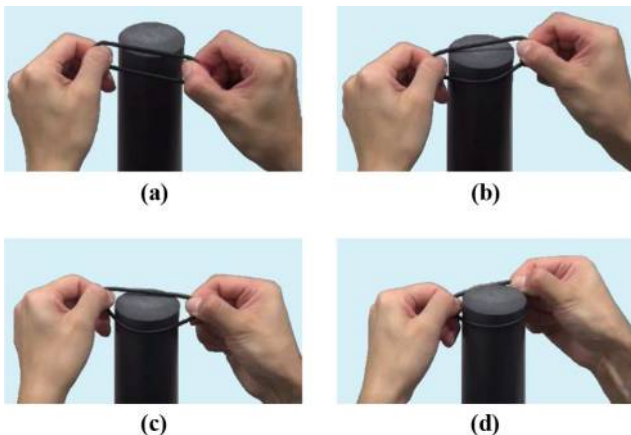
Received 28 December 2016  
Revised 13 June 2017  
17 August 2017  
20 September 2017  
Accepted 31 October 2017

The goal of this work is to develop a planner that is able to automatically plan the motion for a dual-arm manipulator that inserts an elastic object into a cylinder. To achieve this goal, we have to solve the following two problems: first, to accomplish the assembly of a ring-shaped elastic object as shown in Figure 1, a series of key poses for a robot has to be determined; we call this process “assembly task planning”. Second, we have to plan the motion of the robot connecting each pair of key poses, and we call this process “assembly step planning”. For the latter problem, we considered a motion planner based on optimization techniques.

Zucker *et al.* (2013) proposed an algorithm called covariant Hamiltonian optimization and motion planning (CHOMP) based on the gradient descent optimization technique where the choice of the objective function and the terminal condition of the optimization process is free. Thus, it can be expected that the motion planning for manipulating elastic objects with complex deformations could be easily achieved by adding an elastic energy-related term to the objective function of CHOMP. Like this, it would be relatively simple to obtain an optimized path over different cost functions (collision, smoothness, elastic energy of the object, etc.) rather than using sampling-based path planning methods where the path obtained is asymptotically optimal (Karaman and Frazzoli, 2011). Taking into account computational costs, the CHOMP algorithm is more efficient in the time spent per iteration than stochastic optimization planners such as STOMP (Kalakrishnan *et al.*, 2011), which is convenient if the optimization function is non-differentiable or non-smooth.

In our previous work, we proposed an object’s elastic energy-related term (included into the optimization problem of CHOMP) for the motion planning of a two-arm robot toward the insertion of an elastic ring-shaped object into a cylinder (Ramirez-Alpizar *et al.*, 2014). We also introduced a less strict collision cost function than that originally proposed by Zucker *et al.* (2013), which is necessary to allow the manipulator to be as near as possible to the cylinder without colliding with it. In addition, we presented a simulation analysis of the objective functional weights. Extending our previous work, in this paper, we first introduce an assembly task planning algorithm that

**Figure 1** Assembly process of a ring-shaped deformable object performed by a human in four steps: (a) Step 1, (b) Step 2, (c) Step 3 and (d) Step 4



focuses on how to successfully assemble a ring-shaped object to a cylinder without using visual feedback, reducing the computational cost of our assembly planner. This simple search algorithm computes the next feasible key pose (partial goal configuration) of the manipulator’s gripper, taking into consideration the object’s deformation and the position/orientation of the robot’s end effector at each assembly step, avoiding the accumulation of possible positioning errors. In addition to the simulation analysis showing the influence of the optimization weights, we show the experimental results carried out on a Baxter Research Robot[2] using a common rubber band, a silicon-made o-ring and a nitrile-made o-ring to demonstrate the validity of the proposed assembly planner.

This paper is organized as follows: in Section 2, we briefly review related work. In Section 3, we give the outline of the assembly problem discussed in this work. In Section 4, we introduce the planning algorithm for the assembly task of a ring-shaped object into a cylinder. In Section 5, we give a brief introduction to the CHOMP algorithm and introduce an energy-based objective functional to minimize the deformation of the object. In Section 6, we show the simulation results of the proposed assembly planner. In Section 7, we show the experimental results of assembling three different ring-shaped objects using the Baxter robot. In Section 8, we give the conclusion of this work.

## 2. Related work

### 2.1 Motion planning

Motion planning has been a very active research area in robotics in the past decades. Among the most popular algorithms are probabilistic road maps (Karaman and Frazzoli, 2011), rapidly exploring random trees or RRT (LaValle and Kuffner, 2001), the RRT\* (Karaman and Frazzoli, 2010) among others. In contrast, optimization-based planners such as CHOMP (Zucker *et al.*, 2013) and STOMP (Kalakrishnan *et al.*, 2011) have been developed to tackle smoothness problems when using sampling-based planners. More recently, Shoushtari *et al.* (2016) proposed a motion planner using a bio-mimetic approach, where human arm movements are taken into account to generate the motion control of a redundant manipulator. For an extensive review on robot motion planning approaches, the reader is referred to Masehian and Sedighzadeh’s (2007) review.

### 2.2 Manipulation of deformable objects

Toward the challenging topic of manipulating deformable objects, different work has been done, particularly for flexible linear objects, such as ropes and cables. Yamakawa *et al.* (2010) have discussed the motion planning for knotting linear flexible objects, where a model for the linear object is derived and used for the motion planning of the robot to dynamically knot the object and for the deformation control of a flexible rope (Yamakawa *et al.*, 2012). Wakamatsu *et al.* have discussed manipulation plans for knotting and unraveling linear objects by representing the object as a series of crossing states, and based on these states, the manipulation plan is determined (Wakamatsu *et al.*, 2004; Wakamatsu *et al.*, 2006). Vinh *et al.* (2012) have shown a strategy for knotting a deformable rope using a Wii controller as teaching pennant. Wang *et al.* (2015)

have shown a process to design fixtures to arrange and tighten two types of knots and unknots by three different methods. Saha and Isto (2007) have discussed the motion planning for knotting linear deformable objects (LDOs) around static objects using what they called “topologically biased” probabilistic roadmap in the configuration space of the linear deformable object. Rambow *et al.* (2012) have discussed the task of changing the starting configuration of a deformable tube to a given goal configuration. This is achieved by analyzing a human demonstration of the same task and then transferring it to the robot. Lamiraux and Kavraki (2001) proposed a motion planner based on a probabilistic roadmap (Kavraki *et al.*, 1996) that is able to change the initial configuration of an elastic object into a desired goal configuration under manipulation constraints. Moll and Kavraki (2006) proposed a path planner that computes a stable configuration of deformable linear objects based on a sampling-search method. Bretl and McCarthy (2014) have discussed the quasi-static manipulation of planar elastic rods using a sampling-based planning algorithm similar to the one proposed by Moll and Kavraki (2006) where the planar elastic rod is held by a robotic gripper, and the sampling space is defined as the set of equilibrium configurations of the elastic rod. Most of the work involving deformable objects have only discussed LDOs, i.e. ropes, cables and tubes, ; however, few work have been done on the manipulation planning for ring-shaped deformable objects (Yoshida *et al.*, 2015). While the configuration of LDO objects can be estimated by the position of its ends (two points), the configuration of ring-shaped deformable objects cannot be estimated with the same ease (need more than two points), and it requires more complex methods, such as finite element methods.

### 2.3 Assembly of deformable objects

There has been work specifically discussing assembly tasks for flexible parts, which has mainly focused on the insertion of a flexible beam (Zheng *et al.*, 1991) and a flexible wire (Nakagaki *et al.*, 1997) on a rigid hole. Yue and Henrich (2002) have studied the insertion of a vibrating linear deformable object into a hole by using a force/torque sensor mounted on the robot’s wrist. Wolter and Kroll (1996) have discussed a general assembly task of a toy called “launcher” and focused on the push, pull and knot (form into a loop) of strings. Besides the manipulation of LDOs, Villareal and Asada (1991) have presented a methodology for planning assembly tasks involving compliant parts with bounded geometric uncertainties. Miura and Ikeuchi (1995, 1998) have discussed the assembly of a rubber belt and fixed pulleys, where a rubber belt is inserted into a small pulley and then the belt is stretch so as to be inserted into a bigger pulley. However, as far as we know, there has been no work discussing the assembly planning for the insertion of ring-shaped elastic objects, a task that is done by humans and is frequently used by the manufacturing industry, as explained in Section 1.

### 3. Problem formulation

Consider the assembly motion planning of a ring-shaped elastic object into a cylinder, as shown in Figure 1. A cylinder is fixed at the center between both arms of a robot, and the assembly

task starts with the robot holding the object with both grippers. The undeformed diameter of the ring-shaped object is smaller than that of the cylinder, implying that the object must be stretched to be inserted into the cylinder, so as to perfectly fit in the cylinder to avoid any gap (as explained in Section 1). Furthermore, we make the following assumptions:

- The manipulator grasps firmly the elastic object.
- The grasping point of the elastic object with respect to the manipulator’s wrist coordinate system is known and constant.
- The size, shape and Young’s modulus of the object are known.
- The cylinder used for the assembly task is static, rigid and its position and dimensions are known.

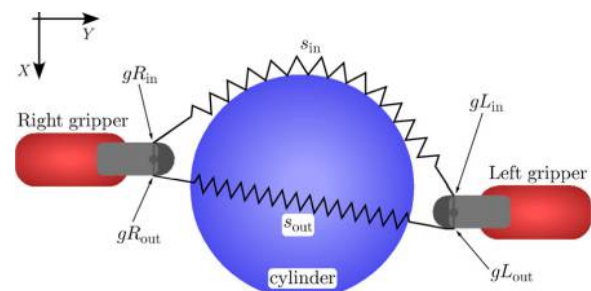
The ring-shaped object is considered as two springs  $s_{in}$  and  $s_{out}$  connected in series (closing the loop), as shown in Figure 2. The connection points are assumed to be at the grasping points by the robot’s grippers such that the undeformed lengths  $l_{0in}$  and  $l_{0out}$  of each of the springs are:

$$l_{0in} = l_{0out} = \frac{1}{2}L_0, \quad (1)$$

where  $L_0 = \pi d_{ring}$ , and  $d_{ring}$  is the undeformed diameter of the ring-shaped object. The shape of the object can be approximated based on an estimation of whether the object has made contact with the cylinder or not. Contact is estimated based on the geometric relationship between the position of the robot’s grippers (grasping points) and the cylinder (a detailed explanation is given in Section 5.2). Once the object’s shape has been approximated, the deformation of each of the springs can be computed, and it can also be evaluated whether the object has been inserted or not into the cylinder.

We divide the assembly motion planning in two procedures: the first one will compute a robot’s key pose based on the robot’s grippers position and the object’s deformation, and we call this procedure “assembly task planning” (detailed in Section 4). The second procedure will plan the motion of the robot between its current position and the next key pose computed in the first procedure, and we call it “assembly step planning” (detailed in Section 5). As will be explained in the following section, the assembly task planning procedure is in charge of evaluating and deciding if the assembly process has successfully finished.

**Figure 2** Top view of the modeled ring-shaped object hold by the robot’s grippers





## 4. Assembly task planning

In this section, we explain the assembly method proposed for inserting a ring-shaped elastic object into a cylinder. Similar to the assembly motion done by a human (Figure 1), the robot first approaches a part of the ring-shaped object at one side of the cylinder, then the robot pulls the object and inserts the rest of the object by moving the hands toward the opposite side of the starting position.

We divide the assembly process in several steps where only one of the arms moves at each step, alternating between left and right arms. The assembly task planner will begin a new step by first computing the next key pose for the robot's gripper (beginning with the left arm at Step 1). Then, it will send this key pose to the motion planner (Section 5) which will search for an inverse kinematics solution using the kinematics and dynamics library, then it will compute the path to be executed by the robot and will send back to the assembly task planner – the current position of the robot (after executing the given path). Based on the information received, the assembly task planner will evaluate and decide if the ring-shaped object has been inserted.

### 4.1 Key pose

To determine the next key pose (grasping point  $P_{i+1} \in \mathbb{R}^3$ ) of the gripper at each step, we implemented the procedure described in Algorithm 1 ( $i$ -th step). This procedure is based on the grippers' current positions and the cylinder information which gives robustness to our planner in the sense that even if the gripper does not move to the exact desired position, in the next step, the planner will start from the current position and will not accumulate positioning errors. Algorithm 1 is basically searching for the closest point to move the robot's grippers a given minimum distance. The grasping point of the object by the grippers at the end of step  $i$  is represented by  $P_i$ ,  $z_{\min}$  is the minimal height to ensure the assembly of the object and  $\text{sgn}(n)$  denotes the sign function of  $n$ . The angle  $\alpha$  is the angle in the  $X$ - $Y$  plane between the  $Y$  axis and the line connecting the grasping points of the object by both grippers  $D = \|P_{i+1} - P_i\|$ , as illustrated in Figure 3.

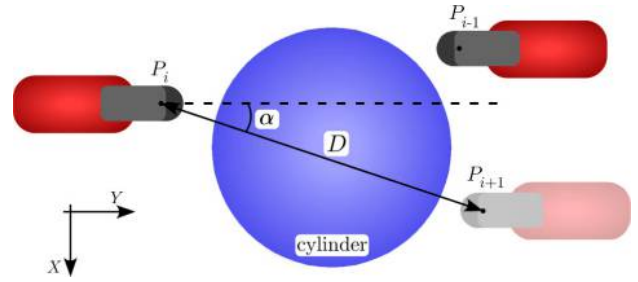
**Algorithm 1** Calculate next key pose

```

1:    $P_{i+1}(x_{i+1}, y_{i+1}, z_{i+1})$ 
2:    $\alpha \leftarrow 0$ 
3:    $D \leftarrow 0.2d_{\text{ring}}$ 
4:   if  $z_i > z_{\min}$  then
5:      $z_{i+1} \leftarrow z_i - dz$ 
6:   else
7:      $z_{i+1} \leftarrow z_i$ 
8:   endif
9:   keep  $\leftarrow$  true
10:  while keep do
11:     $y_{i+1} \leftarrow y_i - (D \cos(\alpha)) \text{sgn}(y_i)$ 
12:     $x_{i+1} \leftarrow x_{i+1} \mid D = \|P_{i+1} - P_i\|$ 
13:    if  $x_{i+1} - x_{i-1} < \Delta X$  or collision
14:      detected or
15:      position is unreachable then
16:        if  $\alpha < \pi/2$  then
17:           $\alpha \leftarrow \alpha + \Delta\alpha$ 
18:        else if  $D < D_{\max}$  then
19:           $D \leftarrow D + \Delta D$ 
20:        else
21:           $\alpha \leftarrow 0$ 

```

**Figure 3** Top view of the cylinder and the robot's grippers at step  $i$



```

19:   else
20:      $y_{i+1} \leftarrow y_{i-1} + \text{sgn}(y_{i-1}) * dy$ 
21:      $x_{i+1} \leftarrow x_{i-1} + dx$ 
22:     keep  $\leftarrow$  false
23:   endif
24:   else
25:     keep  $\leftarrow$  false
26:   endif
27: endwhile
28: return  $P_{i+1}$ 

```

The algorithm starts searching for a key pose ( $P_{i+1}$ ) near to the current position of the opposite gripper ( $P_i$ ). At first, a constant change in the  $z$  coordinate is given ( $dz$ ) to determine  $z_{i+1}$ . Then, as a first try, the value of  $y_{i+1}$  is set such that the line connecting both grippers is parallel to the  $Y$  axis ( $\alpha = 0$  in Figure 3). The initial value of  $D$  is set smaller than the object's undeformed diameter ( $d_{\text{ring}}$ ), and then  $x_{i+1}$  is computed such that  $D = \|P_{i+1} - P_i\|$  is satisfied (Algorithm 1: line 11). The initial value of  $D$  at each step is set depending on the position of the grippers, i.e. at the beginning of the assembly, it is small and as the assembly progresses (the object begins to get deformed), its initial value is changed to  $d_{\text{ring}}$  and finally when it approaches the end of the assembly, its initial value is set again small. Furthermore, the choice of calculating first  $y_{i+1}$  based on  $\alpha$  (in the  $X$ - $Y$  plane) and then  $x_{i+1}$  based on  $D$  is to ensure that the search begins with a valid  $y_{i+1}$  (not in collision with the cylinder) and with the smallest possible value for  $D$  (i.e. smallest deformation of the ring-shaped object).

Next, the algorithm checks three important conditions:

- 1  $P_{i+1}$  is not in collision with the cylinder.
- 2 The robot can reach the position.
- 3  $P_{i+1}$  is at least at a distance  $\Delta X$  from the previous key pose (Algorithm 1: line 12).

If any of these three conditions are not satisfied, the algorithm will increment  $\alpha$ , recompute  $y_{i+1}$  and  $x_{i+1}$  and check again. It will iterate until it finds a point  $P_{i+1}$  satisfying all three conditions. If  $\alpha$  reaches its maximal value  $\pi/2$ , then it will increment  $D$  and reset  $\alpha$  to zero and begin to iterate again. In the extraordinary case that  $D$  also reaches its maximal allowed value  $D_{\max} = 1.2 d_{\text{ring}}$ , the algorithm will stop and will set the next key pose to a close by point in  $X$  positive direction by  $dx$  and in the outward direction from the cylinder by  $dy$  ( $Y$  axis) which should not be in collision with the cylinder (Algorithm 1: lines 20 and 21). The values of  $dx$  and  $dy$  are determined based on the tolerance error of the robot's position controller, otherwise if we choose smaller values than the tolerance error the robot will not move.  $\Delta X$  plays a key role in the number of

steps needed to finish the assembly task, whereas the limits on  $\alpha$  and  $D$  will ensure that the object's deformation does not go beyond  $1.2 d_{\text{ring}}$  and that the assembly task is achieved successfully.

#### 4.2 Assembly ending condition

At the end of each executed step, the assembly task planner will check if the ring-shaped object has been inserted. Based on the position of both grippers and under Assumption 1 of Section 3, it is possible to assess (with a certain degree of confidence) if the ring has been inserted by checking if there are intersecting points between the line connecting the outside grasping points  $gR_{\text{out}} gL_{\text{out}}$  (Figure 2) and the cylinder. If an intersecting point exists, it is determined that the object has not been inserted, and the task planner proceeds to compute a new key pose. Otherwise, it will check the  $x$  and  $z$  components of  $gR_{\text{out}} gL_{\text{out}}$  to determine if the assembly is starting or is ending. This method is valid because we do not move both arms at the same time. By moving one arm at a time it is possible to assume that the robot will follow certain trajectory (given the "naive" initialization of the CHOMP algorithm). Therefore, given the trajectory in  $z$  direction of the grasping points, it is possible to make an educated guess that the object has been "caught" in the cylinder when the grasping points are below the cylinder's surface and ahead (in  $x$ ) of its center.

### 5. Assembly step planning

In this section, we describe the motion planner used to obtain the trajectory between the key poses computed by the assembly task planner explained in Section 4.

#### 5.1 Covariant Hamiltonian optimization and motion planning algorithm

In this section, we propose a motion planning algorithm for manipulating elastic objects, based on the algorithm developed by Zucker *et al.* (2013), called CHOMP. This algorithm is capable of finding a smooth and collision-free trajectory  $\xi$  between two specific configurations  $q_0$  and  $q_{\text{goal}}$  of the configuration space  $\mathbb{R}^m$ . The trajectory  $\xi$  is expressed as a function mapping time to robot configurations  $q \in \mathbb{R}^m$ . Using a uniform discretization of  $n$  time steps of length  $\Delta t$ , the trajectory is represented as  $\xi \approx (q_1^T, q_2^T, \dots, q_n^T)^T \in \mathbb{R}^{n \times m}$ . The CHOMP algorithm typically starts with a simple straight line between the given configurations (even if it is not collision-free), as the initial trajectory  $\xi_0$ . Then, it optimizes the initial trajectory through an iterative update rule (Zucker *et al.*, 2013) given by:

$$\xi_{i+1} = \xi_i - \frac{1}{\eta} (K^T K)^{-1} \bar{\nabla} U(\xi_i) \quad (2)$$

where  $\xi_i$  is the refined trajectory at iteration  $i$ ,  $K$  is a finite differencing matrix,  $\eta$  is the regularization coefficient that determines the trade-off between minimizing the objective functional  $U$  and the step size and  $\bar{\nabla}$  is the functional gradient operator. The objective functional  $U(\xi_i)$  is given by:

$$U(\xi) = \mathcal{F}_{\text{obs}}(\xi) + \lambda \mathcal{F}_{\text{smooth}}(\xi) \quad (3)$$

where  $\mathcal{F}_{\text{smooth}}$  is the smoothness objective that penalizes the trajectory  $\xi_i$  based on dynamical parameters such as the

squared velocity norms over the trajectory, and  $\mathcal{F}_{\text{obs}}$  is the obstacle objective which penalizes the robot for being near and/or in contact with the environment and/or itself.

#### 5.2 Energy objective functional

In this work, we use CHOMP for the assembly manipulation of a ring-shaped elastic object. We suppose the assembly task shown in Figure 1. The objects used in this kind of assembly process, usually have a relatively high stiffness[3], which as explained in Section 1, have two important implications when assembling them. First, large deformations lead to its deterioration and/or fracture, e.g. the o-ring is not able to return to its original size, thus generating undesired gaps with the cylinder. Second, a considerable amount of force is needed to generate large deformations. Thus, it is very important to keep the object's deformation as small as possible. To minimize the object's deformation, we introduce an energy objective functional that penalizes the trajectory  $\xi_i$  for stretching the object. Therefore, we rewrite the objective functional of (3) as:

$$\mathcal{U}(\xi) = w_c \mathcal{F}_{\text{obs}}(\xi) + w_s \mathcal{F}_{\text{smooth}}(\xi) + w_e \mathcal{F}_{\text{energy}}(\xi) \quad (4)$$

where  $w_c$ ,  $w_s$ ,  $w_e$  are the weights of the obstacle objective, the smoothness objective and the energy objective, respectively. We use the smoothness objective as define by Zucker *et al.* (2013) and the obstacle objective as described in Section 5.3. We define the energy objective functional  $\mathcal{F}_{\text{energy}}$  as:

$$\mathcal{F}_{\text{energy}}(\xi) = \int_0^1 U(\xi(t)) \left\| \frac{d}{dt} \xi(t) \right\| dt \quad (5)$$

where  $U(\xi)$  is the energy cost function in the configuration space.

The functional gradient (Quinlan, 1994) of the energy objective is obtained as:

$$\bar{\nabla} \mathcal{F}_{\text{energy}}(\xi) = \|\xi'\| \left( (I - \hat{\xi}' \hat{\xi}'^T) \nabla U - U \kappa \right) \quad (6)$$

where  $\kappa$  is the curvature vector (Quinlan, 1994) given by:

$$\kappa = \frac{1}{\|\xi'\|^2} (I - \hat{\xi}' \hat{\xi}'^T) \xi'',$$

$\nabla U = \partial U / \partial \xi$  is the gradient of  $U$ , and  $\xi'$  and  $\hat{\xi}$  denote the time derivative and the normalized vector of  $\xi$ , respectively.

As mentioned in Section 1, one important advantage of using optimization methods for motion planning is the free choice of the cost function. Consequently, for the energy cost function  $U(\xi)$ , we use the potential energy of a spring:

$$U(\xi) = \frac{1}{2} k x_d(\xi)^2 \quad (7)$$

where  $k$  is the ideal stiffness of the spring, and  $x_d(\xi)$  is the deformation of the spring. In this case, we approximate the stiffness of the ring-shaped object through its Young's modulus (tensile stress by tensile strain)  $E$  as:

$$k = \frac{EA_0}{L_0} \quad (8)$$

where  $A_0$  and  $L_0$  are the cross-sectional area and the length of the undeformed object, respectively.

### 5.2.1 Object's deformation

The deformation of the object  $x_d$  is approximated as:

$$x_d = l_{in} + l_{out} - L_0, \quad (9)$$

where  $l_{in}$  and  $l_{out}$  are the length of the springs  $s_{in}$  and  $s_{out}$  (Figure 2), respectively.

As discussed in Section 4.2, the deformation of the object is computed under the assumption that the object gets ‘‘caught’’ in the cylinder when the grasping points are below the cylinder's surface and ahead (in  $x$ ) of its center. First it is checked if the object has been stretched by verifying if:

$$2(\|P_{i+1} - P_i\| + g_w) > L_0, \quad (10)$$

where  $g_w$  is the width of the gripper at the grasping point. If the object is being stretched, then it is determined if  $s_{in}$  has made contact with the cylinder by checking if there are intersecting points between the line connecting the inside grasping points  $gL_{in}$ ,  $gR_{in}$  (Figure 2) and the cylinder. If there are no intersecting points, it is considered that there is no contact between  $s_{in}$  and the cylinder, thus:

$$l_{in} = \|gR_{in} - gL_{in}\| + g_w. \quad (11)$$

In the case where there are intersecting points, it is determined that  $s_{in}$  has made contact with the cylinder and the corresponding contact points ( $pc_1, pc_2 \in \mathbb{R}^3$ ) are computed. Because it is already known that the object has been stretched, we know that the lines between the inside grasping points and the contact points are tangent lines to the cylinder (at  $pc_1, pc_2$ ). Thus, we can approximate the length of  $s_{in}$  as:

$$l_{in} = \|gR_{in} - pc_2\| + \|gL_{in} - pc_1\| + l_{arc} + g_w, \quad (12)$$

where  $l_{arc}$  is the arc length between the contact points  $pc_1$  and  $pc_2$ .

Similar to  $s_{in}$ , it is determined if  $s_{out}$  is in contact with the cylinder. If there are no intersecting points between the cylinder and the line connecting the outside grasping points  $gL_{out}$ ,  $gR_{out}$  or if these are above the surface of the cylinder, it is considered that there is no contact between  $s_{out}$  and the cylinder, and thus:

$$l_{out} = \|gR_{out} - gL_{out}\| + g_w. \quad (13)$$

Otherwise, the intersecting points ( $pc_3, pc_4 \in \mathbb{R}^3$ ) are computed. Depending on the height  $z$  of  $gR_{out}$  and  $gL_{out}$  it is determined if  $s_{out}$  has made contact with the cylinder and in how many points ( $n$ ). Finally,  $s_{out}$  is segmented in  $n + 1$  lines and we can approximate the length of  $s_{out}$  as:

$$l_{out} = g_w + \sum_{j=1}^{n+1} l_{s_j}, \quad (14)$$

where  $l_{s_j}$  is the length of the  $j$ -th segment of  $s_{out}$ . Like this, the deformation of the ring-shaped object is approximated by

computing the deformations of springs  $s_{in}$  and  $s_{out}$  based only in the position of the grasping points and the cylinder.

### 5.3 Collision cost function

Next, we consider modifying the collision cost function such that the CHOMP algorithm can be used for the assembly motion planning of elastic parts. The obstacle objective in equation (4) is given by (Zucker *et al.*, 2013):

$$\mathcal{F}_{obs}(\xi) = \int_0^1 \int_{\mathcal{B}} c(x(\xi(t), u)) \left\| \frac{d}{dt} x(\xi(t), u) \right\| du dt, \quad (15)$$

where  $\mathcal{B} \subset \mathbb{R}^3$  is the set of points on the exterior body of the robot, and  $x$  denotes the forward kinematics mapping a robot configuration  $q$  and a particular body point  $u$  to a point  $x(q, u)$  in the workspace, and  $c$  is a workspace collision cost function that penalizes the robot for being inside or near the environment given as:

$$c(x) = \begin{cases} -d(x) + \frac{1}{2}\varepsilon, & \text{if } d(x) < 0 \\ \frac{1}{2\varepsilon}(d(x) - \varepsilon)^2, & \text{if } 0 \leq d(x) \leq \varepsilon \\ 0, & \text{otherwise} \end{cases} \quad (16)$$

where  $d(x)$  is the distance from a point  $x$  to the boundary of the nearest obstacle, and  $\varepsilon$  is the collision threshold. Here, we would like to emphasize that the collision cost function is given in the workspace, because it evaluates the distance between a robot's body part and the environment. However, in the case of the energy cost in equation (7), as we seek to minimize the object's deformation, we use the configuration space to directly obtain the position of both grasping points and evaluate the object's deformation.

In Section 6, we will show that using the collision cost function given by equation (16), indeed, a collision free trajectory is obtained. However, this collision cost pushes away the trajectory needlessly far from a possible collision with the environment (cylinder), thus stretching the ring-shaped object more than two times its original size which may result in the undesired release of the ring-shaped object and in the assembly task failure.

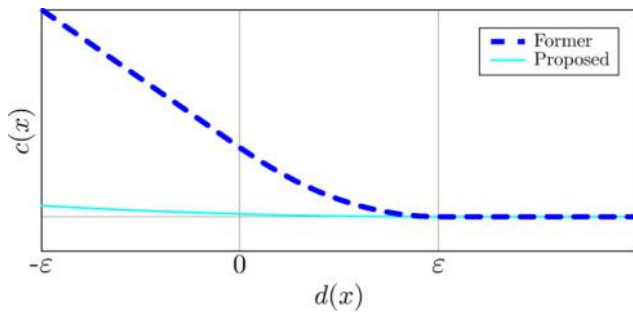
In our case, as we want to avoid collisions with the environment and at the same time minimize the deformation of the elastic object, we need to have a balance between the collision cost function and the energy cost function (Section 5.2). For this reason, we define the collision cost function as follows:

$$c(x) = \begin{cases} \frac{1}{2}\varepsilon(d(x) - \varepsilon)^2, & \text{if } d(x) < d_{clear} \\ 0, & \text{otherwise} \end{cases} \quad (17)$$

where we define  $d_{clear}$  as the minimum distance between the boundary of a body point and the boundary of the nearest obstacle, before being in collision. With this collision cost function, the robot is able to move as near as allowed by  $d_{clear}$  to the environment.

Figure 4 shows the plot of the original collision cost function given by equation (16) and the plot of the proposed collision cost function given by equation (17); for a fair comparison, we

**Figure 4** Comparison between collision cost functions  $c(x)$ , when  $d_{\text{clear}} = \varepsilon$



let  $d_{\text{clear}} = \varepsilon$ . Note that if  $d_{\text{clear}} < \varepsilon$ ,  $c(x)$  will become zero faster, but the rest of the function is the same as the one depicted in Figure 4. It can be seen that the original cost function rapidly increases as the distance to the obstacle gets smaller, whereas the proposed cost function increases with a difference of  $1/\varepsilon^2$  times the original one (when  $d(x) < 0$  and  $\varepsilon < 1$ ). Therefore, even for very small values of  $\varepsilon$  (e.g.  $1 \times 10^{-6}$ ), the value of  $c(x)$  when  $d(x) > 0$  will not change significantly. Only when the robot is not in collision ( $d(x) > 0$ ), we could get similar values of  $c(x)$  for the original cost function using small values of  $\varepsilon$  and the proposed one.

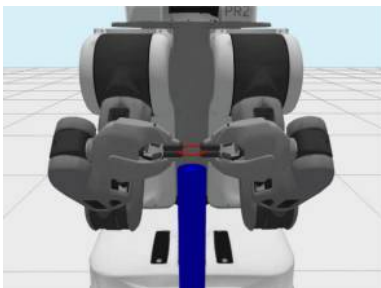
### 6. Simulation analysis

In this section, we present the simulation analysis conducted to demonstrate the validity of our assembly planner. First, we make a brief description of the simulation environment used and then we discuss the influence of the objective functionals' weights in equation (4).

#### 6.1 Simulation setting

The robot operating system platform and the Gazebo simulator are used to carry out the simulation of the PR2 robot handling an elastic object (approximated by rigid cylindrical links connected by rotational and translational joints). We consider the assembly of a ring-shaped object into a cylinder located at the center between the arms of the robot. Figure 5 shows the initial state from which the assembly process starts. The ring-shaped elastic object has an inner radius of 49.9 mm, a thickness of 3 mm and a Young's modulus of  $E = 4.125$  MPa. The cylinder has a radius of 50 mm [4]. Also, we added a condition to the step planner (CHOMP algorithm) to be able

**Figure 5** Initial state of the PR2 robot in simulation



to “always” obtain a collision-free trajectory. Therefore now, the step planner will discard those trajectories with smaller costs that are in collision and will only consider collision-free trajectories.

Figure 6 shows the simulation results of the assembly process carried out using the proposed assembly planner, where each snapshot shows the achieved position at each assembly step by the PR2 robot. The assembly process is accomplished in six steps for  $\Delta X = 0.02$  and  $dz = 0.007$  in the assembly task planner, and it begins by moving the left arm at Step 1 [Figure 6(a)] and finishes with the right arm at Step 6 [Figure 6(f)].

To discuss the importance of the collision cost function, we set  $w_c = 0$  in equation (4) (no consideration of the object's deformation). Figure 7 shows the top view ( $X$ - $Y$  plane) in (a) and the front view ( $Y$ - $Z$  plane) in (b), of the trajectory described by the grasping position of the left gripper during Step 3 of the assembly process, where the shaded area represents the cylinder. In Figure 7, we compare the trajectory obtained using the original CHOMP's collision cost in equation (16) which we call “former” (dashed line), and the trajectory obtained using equation (17) which we call “proposed” (continuous line). As a first attempt we choose a collision weight of  $w_c = 10.0$  which yields a collision cost smaller than the original one. It can be seen that the grasping position trajectory obtained from the original CHOMP makes a big turn around the cylinder, whereas the trajectory obtained through the proposed collision

**Figure 6** Assembly process in simulation at (a) end of Step 1, (b) end of Step 2, (c) end of Step 3, (d) end of Step 4, (e) end of Step 5 and (f) end of Step 6

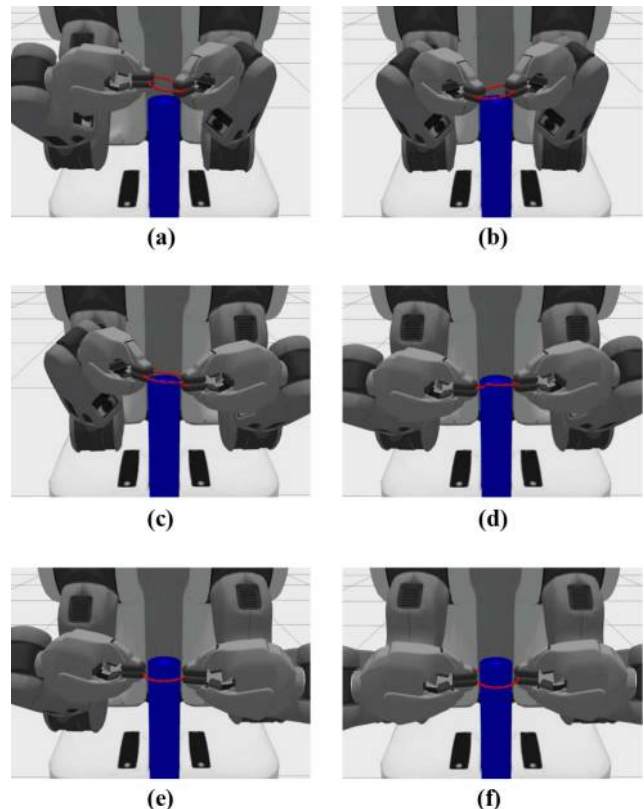
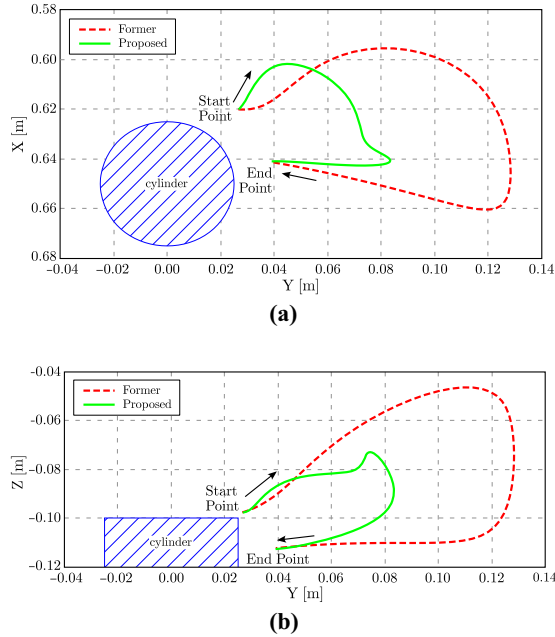




**Figure 7** Robot's left gripper trajectory (at the grasping point during Step 3), obtained with the original CHOMP's collision cost function given by equation (16) and the proposed collision cost given by equation (17)



**Notes:** In (a) The  $X$ - $Y$  plane; (b) the  $Y$ - $Z$  plane

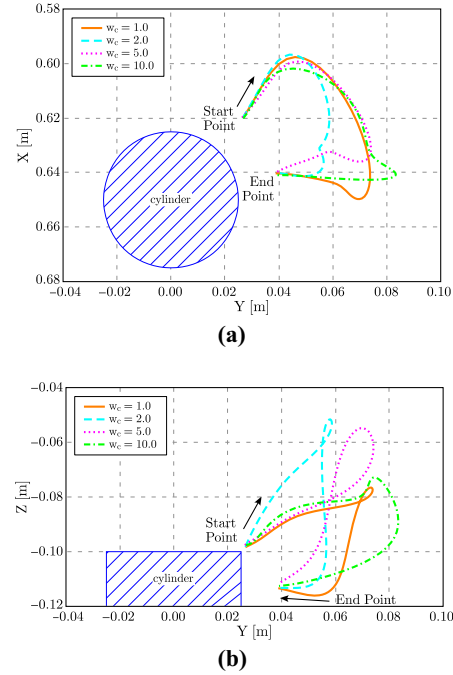
cost function considerably shortens the turn around the cylinder. We must point out that for some of the assembly steps, when the given goal position for the gripper is very close to the cylinder, the original CHOMP was not able to yield a collision-free trajectory (using the same collision threshold  $\varepsilon$  and the same number of allowed iterations), because pulling the trajectory far from the object implies a considerable increase in the length of the trajectory therefore increasing its cost. In contrast, with the proposed collision cost we were able to get a collision-free trajectory, as the proposed cost function pulls the trajectory by a smaller amount at each iteration, keeping the length of the trajectory smaller. Despite this, the average number of iterations needed was the same or less than with the original CHOMP.

### 6.2 Analysis of objective functionals' weights

Next, we analyzed the influence of the collision weight cost  $w_c$  in the resulting trajectory ( $w_e = 0$ ). Figure 8 shows the top view ( $X$ - $Y$  plane) in (a) and the front view ( $Y$ - $Z$  plane) in (b) of the trajectories described by the grasping position of the left gripper during Step 3 of the assembly process, obtained with four different collision weights  $w_c$ . It can be seen that the trajectories are similar for all the values of  $w_c$ . Their collision costs, given by equation (15), are also similar (within 0.0001).

Figure 9 shows the top view ( $X$ - $Y$  plane) in (a) and the front view ( $Y$ - $Z$  plane) in (b), of the trajectories described by the grasping position of the left gripper, obtained with the proposed collision cost function ( $w_e = 0$ ) and obtained when adding the energy objective functional to the step planner ( $w_e \neq 0$ ). As it can be seen, the trajectories obtained when  $w_e \neq 0$  are

**Figure 8** Robot's left gripper trajectory (at the grasping point during Step 3) using the proposed collision cost function for four different collision weights



**Notes:** In (a) The  $X$ - $Y$  plane; (b) the  $Y$ - $Z$  plane, for  $w_e = 0$

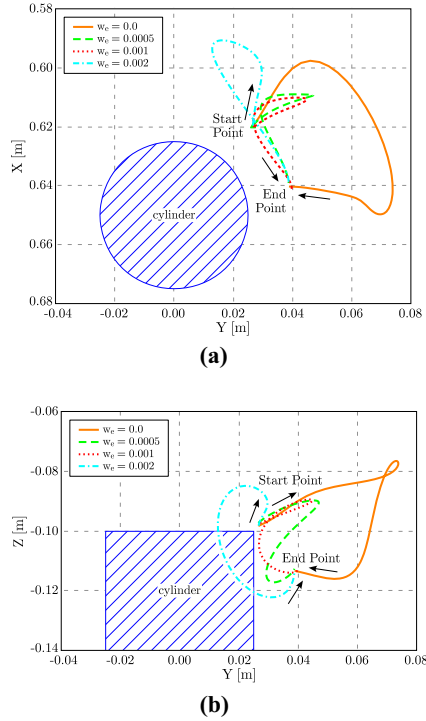
considerably shorter and closer to the cylinder than the one with  $w_e = 0$ .

Similarly, Figure 10 shows the top view ( $X$ - $Y$  plane) in (a) and the front view ( $Y$ - $Z$  plane) in (b), of the trajectories described by the grasping position of the right gripper during Step 4 of the assembly process, obtained with the proposed collision cost function ( $w_e = 0$ ) and obtained when adding the energy objective functional to the step planner ( $w_e \neq 0$ ). At this assembling step, it can be seen that the trajectory obtained with  $w_e = 0.0005$  describes a semicircle just as if it was passing along the cylinder's edge, consequently minimizing the object's deformation. In contrast, the trajectory obtained with  $w_e = 0$  makes a turn around the cylinder in a similar way to the trajectory at Step 3 (Figure 9). Similar to the case shown in Figure 9, for  $w_e = 0.001$  and  $0.002$ , the gripper moves toward the robot, avoiding the cylinder and getting closer to the opposite gripper, reducing the deformation of the elastic object.

For analyzing the influence of the objective functionals weights, several simulations were carried out. The average sum of all the collision costs [equation (15)] and all the energy costs [equation (5)] for all the steps of the assembly process (the average cost of three simulation runs for each combination of weights) are summarized in Table I for  $w_e = 0.0005$ , Table II for  $w_e = 0.001$  and Table III for  $w_e = 0.002$ . The smoothness costs are not included as they are in the order of hundreds of thousands. Furthermore, the largest difference among them is 0.25 per cent of the overall average cost, which means there is no significant difference among them. It can be seen that overall the smallest energy costs were obtained with  $w_e = 0.002$ ,



**Figure 9** Robot’s left gripper trajectory (at the grasping point during Step 3) using the proposed step planner with and without the energy objective functional



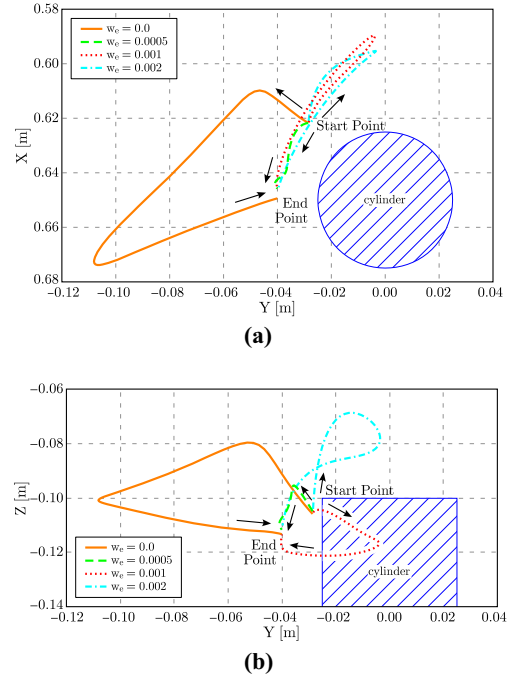
**Notes:** In (a) The  $X$ - $Y$  plane; (b) the  $Y$ - $Z$  plane, with  $w_s = 0.00001$  and  $w_c = 1.0$

whereas the collision costs do not change significantly. The smallest energy cost was obtained for the combination of  $w_c = 0.002$  with  $w_c = 2.0$  and  $w_s = 0.00001$ . If we group the results by  $w_s$  instead of  $w_c$  and calculate the average energy cost, it is found that the smallest energy costs were obtained with  $w_s = 0.00001$ . Similarly, if we group by  $w_c$ , it is found that the smallest energy costs were obtained with  $w_c = 2.0$ . These results coincide with the smallest energy cost obtained.

### 7. Experimental results

In this section, the experimental results of the proposed assembly planner using a Baxter robot are presented. For validating the proposed assembly planner, we used the ring-shaped elastic objects shown in Figure 11. The first object is a common rubber band (natural rubber), the second is an o-ring made of silicon rubber (stiffer than the rubber band) and the third is an o-ring made of nitrile rubber (also known as NBR) commonly known as a packing, which is stiffer than both the rubber band and the silicon made o-ring. Their dimensions are summarized in Table IV. The parameters given to both the sequence planner and the CHOMP algorithm are those of the nitrile-made o-ring (the stiffer of the three objects) that has a Young’s modulus of  $\approx 4.125$  MPa (based on the o-ring’s manufacturer data sheet). The parameters used in the assembly task planner are  $dz = 0.007$  and  $\Delta X = 0.03$  m and the cylinder’s diameter is 5.0 cm. For comparison purposes, the joints’ trajectories requested to the robot are exactly the same for all

**Figure 10** Robot’s right gripper (at the grasping point during Step 4) using the proposed step planner with and without the energy objective functional



**Notes:** In (a) The  $X$ - $Y$  plane; (b) the  $Y$ - $Z$  plane, with  $w_s = 0.00001$  and  $w_c = 1.0$

**Table I** Collision cost and energy cost for  $w_e = 0.0005$

$w_s$	$w_c$	Collision cost	Energy cost
0.000005	0.5	0.0162	17.14
	1.0	0.0133	25.92
	2.0	0.0135	22.91
0.00001	0.5	0.0165	21.40
	1.0	0.0136	20.92
	2.0	0.0140	20.04
0.00002	0.5	0.0155	18.34
	1.0	0.0141	22.51
	2.0	0.0149	25.06
Average		0.0146	21.58

the three objects, i.e. we only plan once (for the stiffest object, the nitrile-made o-ring) and then use the same plan for all the objects. Figure 12 shows the snapshots of the experiments using the rubber band. The robot accomplishes the assembly task in 24 s (humans can do it in 5 s), when using a discretization time of  $\Delta t = 0.01$  and a trajectory length of 3 s in the CHOMP algorithm (Section 5.1), the execution time can be shortened if we use a smaller trajectory length. Also, it was verified that the robot successfully assembled all of the ring-shaped objects into the cylinder. These results suggest that by supposing that the object has a high stiffness (for the energy cost computation purposes in the CHOMP algorithm), the obtained motion plan can work for objects with equal or less stiffness than the supposed one. Thus, we can drop out the

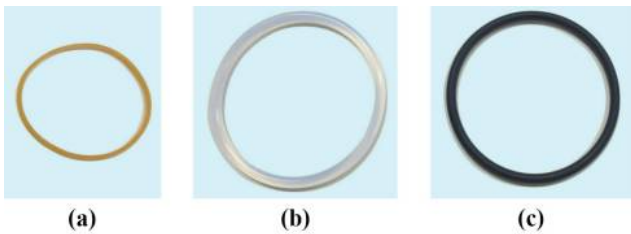
**Table II** Collision cost and energy cost for  $w_e = 0.001$

$w_s$	$w_c$	Collision cost	Energy cost
0.000005	0.5	0.0153	19.42
	1.0	0.0180	15.94
	2.0	0.0142	17.90
0.00001	0.5	0.0141	20.21
	1.0	0.0153	16.20
	2.0	0.0144	15.67
0.00002	0.5	0.0150	20.99
	1.0	0.0155	19.73
	2.0	0.0136	26.60
Average		0.0150	19.18

**Table III** Collision cost and energy cost for  $w_e = 0.002$

$w_s$	$w_c$	Collision cost	Energy cost
0.000005	0.5	0.0154	18.75
	1.0	0.0142	17.74
	2.0	0.0167	15.33
0.00001	0.5	0.0155	17.83
	1.0	0.0155	17.16
	2.0	0.0170	15.22
0.00002	0.5	0.0163	16.88
	1.0	0.0161	21.25
	2.0	0.0158	16.47
Average		0.0158	17.40

**Figure 11** O-Ring shaped objects used in experiments



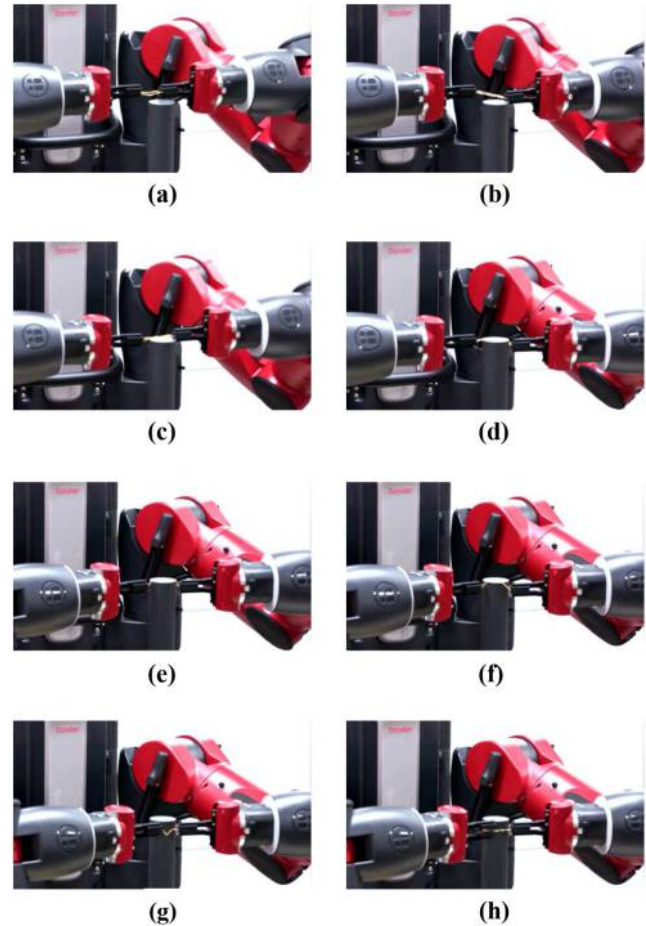
**Notes:** (a) A rubber band made of natural rubber; (b) an o-ring made of silicon rubber; (c) an o-ring made of nitrile rubber

**Table IV** Dimensions of the objects shown in [Figure 11](#)

Object	Undeformed inner diameter (mm)	Thickness (mm)
Rubber band	47.0	1.0
Silicon o-ring	49.7	3.5
Nitrile o-ring	49.4	3.0

assumption of knowing the material of the ring-shaped object and set the value of  $k$  through [equation \(8\)](#) using the Young's modulus of a known material with high stiffness. Also, it can be seen that through the entire assembly process the position of the grasping point of the object does not change significantly supporting our assumption that the robot grasps firmly the

**Figure 12** Snapshots of the experiment using a rubber band at (a) initial state, (b) end of Step 1, (c) end of Step 2, (d) end of Step 3, (e) end of Step 4, (f) end of Step 5, (g) end of Step 6 and (h) after releasing the object

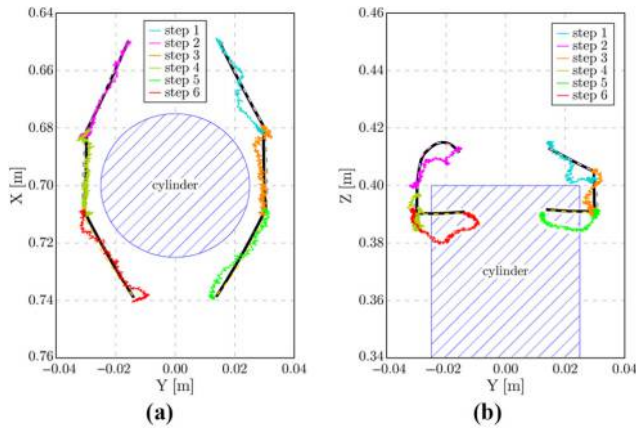


object. It should be noticed that this assumption is merely for the sake of simplicity in the computation of the object's deformation in the CHOMP algorithm. However, it does not affect the performance of the assembly planner as verified through the experiments.

[Figure 13](#) shows the trajectories of each of the tips of the robot's grippers in experiment (using the rubber band) and simulation compared with the desired trajectories, where the continuous, dashed and bold lines represent the experimental, simulation and desired trajectories, respectively. In this case, as it can be seen the robot's tip trajectories followed the desired ones, successfully assembling the rubber band into the cylinder. Furthermore, in this work, we set the cylinder vertically; nevertheless, it can also be set horizontally or in any other posture (reachable by the robot). The only modification needed would be the transformation between the coordinate system used now and the new posture, without affecting anything else.

We repeated the experiment with both the rubber band and the silicon-made o-ring five times in a row with each material, having succeeded in the assembly each time. In contrast with

**Figure 13** Tip trajectories of Baxter’s grippers when the object is the rubber band



**Notes:** In (a) top view ( $X$ - $Y$  plane) and in (b) front view ( $Y$ - $Z$  plane). The continuous, dotted and dashed lines represent the experimental data, simulation data and the desired trajectories, respectively

the nitrile-made o-ring, we were able to do the experiment only two times in a row, because in the second time the designed holder (shown in Figure 14) for grasping the o-ring got detached from the robot’s finger. This happened due to the high stiffness of the o-ring, however although the holder got detached at the last step, the o-ring was correctly inserted in the cylinder. Figure 15 shows the average of the computed deformation of the object (using the method presented in Section 5.2) in all of the experiments (five times for the rubber band and the silicon-made o-ring and two times for the nitrile-made o-ring). It can be seen that for the first steps the assembly planner is able to keep the object undeformed. Then as the object begins to be inserted (taking the shape of the cylinder), it begins to deform. At the end, it can be observed that the rubber band being the less stiffer and having the shortest perimeter, gets deformed more than the o-rings. At the last step, it can be seen that the deformation of the o-rings is very similar, which means that their shape is about the same (inserted on the cylinder).

### 8. Conclusion

This paper discussed the assembly planning of ring-shaped elastic objects considering the object’s deformation. The main results of this paper are summarized as follows:

**Figure 14** Robot holding the silicon-made o-ring using the designed holder

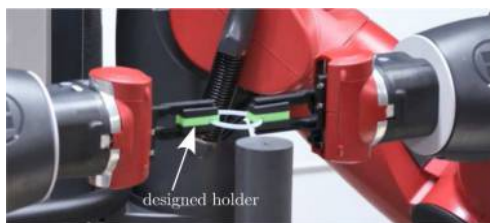
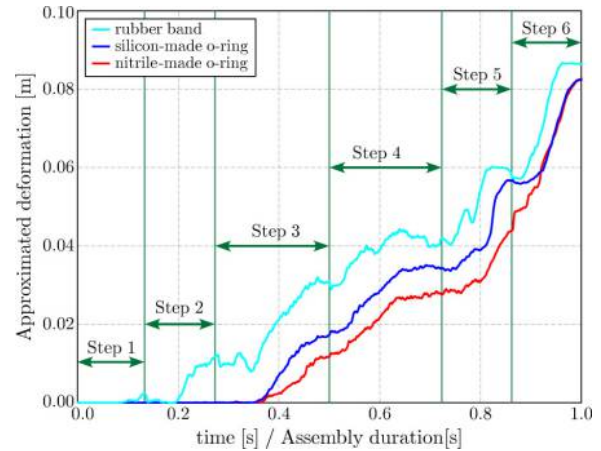


**Figure 15** Average of the computed deformation of each of the objects in experiments



- We presented an assembly task planner for a dual-arm robot that computes key poses of the robot to successfully accomplish the assembly task of a ring-shaped object into a cylinder.
- We introduced an energy objective functional that minimized the deformation of the elastic object when manipulated by a dual-arm robot.
- We introduced a less strict collision cost function that allows the robot to be near to its environment without colliding. This function proved that it can yield collision-free trajectories.
- We showed that the addition of the energy-based objective functional to the original CHOMP method is effective for minimizing the elastic energy of the object through several simulations.
- We examined the influence of the objective functionals weights, and found that for the smoothness and collision costs there are no significant differences. In contrast, for the energy cost, a combination of weights yielding the smallest energy cost was found.
- We confirmed the validity of the proposed assembly planner through experiments using three different elastic ring-shaped objects.

This work is considered to be the basis for accomplishing other types of assembly tasks involving deformable objects. In the future we would like to discuss assembly tasks that required the ring-shaped object to be placed in a specific part of the cylinder and/or on another object and how to pick/grasp the ring-shaped objects autonomously. Also, we would like to discuss other methods to achieve the assembly task of elastic objects that have different shapes.

### Notes

- 1 NASA’s space shuttle *Challenger* explosion in 1986 was determined to be due to an o-ring failure (Atkinson, 2012).
- 2 [www.rethinkrobotics.com/baxter/](http://www.rethinkrobotics.com/baxter/)
- 3 We refer to stiffness as the state of being difficult to bend or stretch.



4 In this particular case the difference between the cylinder's diameter and the ring's one is 0.1 mm. Nevertheless, for larger differences it can be expected that the assembly process would need more steps to be accomplished, as the number of steps depends on the diameters of both the object and the cylinder.

## References

- Atkinson, J. (2012), "Engineer who opposed challenger launch offers personal look at tragedy", *The Researcher News*, National Aeronautics and Space Administration (NASA), available at: [www.nasa.gov/centers/langley/news/researchernews/rn\\_Colloquium1012.html](http://www.nasa.gov/centers/langley/news/researchernews/rn_Colloquium1012.html)
- Bretl, T. and McCarthy, Z. (2014), "Quasi-static manipulation of a Kirchhoff elastic rod based on a geometric analysis of equilibrium configurations", *International Journal of Robotics Research (IJRR)*, Vol. 33 No. 1, pp. 48-68.
- Friedrich, W., Lim, P. and Nicholls, H. (1996), "Sensory gripping system for variable products", *IEEE International Conference on Robotics and Automation (ICRA)*, Minneapolis, MN, Vol. 4, pp. 3324-3329.
- Kalakrishnan, M., Chitta, S., Theodorou, E., Pastor, P. and Schaal, S. (2011), "STOMP: Stochastic trajectory optimization for motion planning", *IEEE International Conference on Robotics and Automation (ICRA)*, Shanghai, pp. 4569-4574.
- Karaman, S. and Frazzoli, E. (2010), "Incremental sampling-based algorithms for optimal motion planning", *Robotics Science and Systems VI*, Vol. 104.
- Karaman, S. and Frazzoli, E. (2011), "Sampling-based algorithms for optimal motion planning", *International Journal of Robotics Research (IJRR)*, Vol. 30 No. 7, pp. 846-894.
- Kavraki, L.E., Svestka, P., Latombe, J.C. and Overmars, M.H. (1996), "Probabilistic roadmaps for path planning in high-dimensional configuration spaces", *IEEE Transactions on Robotics and Automation*, Vol. 12 No. 4, pp. 566-580.
- Lamiroux, F. and Kavraki, L.E. (2001), "Planning paths for elastic objects under manipulation constraints", *International Journal of Robotics Research (IJRR)*, Vol. 20 No. 3, pp. 188-208.
- LaValle, S.M. and Kuffner, J.J. Jr. (2001), "Randomized kinodynamic planning", *The International Journal of Robotics Research*, Vol. 20 No. 5, pp. 378-400.
- Mashian, E. and Sedighzadeh, D. (2007), "Classic and heuristic approaches in robot motion planning—a chronological review", *World Academy of Science, Engineering and Technology*, Vol. 23, pp. 101-106.
- Miura, J. and Ikeuchi, K. (1995), "Assembly of flexible objects without analytical models", *IEEE/RSJ International Conference on Intelligent Robots and Systems (IROS)*, Pittsburgh, PA, Vol. 2, pp. 77-83.
- Miura, J. and Ikeuchi, K. (1998), "Task planning of assembly of flexible objects and vision-based verification", *Robotica*, Vol. 16 No. 3, pp. 297-307.
- Moll, M. and Kavraki, L.E. (2006), "Path planning for deformable linear objects", *IEEE Transactions on Robotics*, Vol. 22 No. 4, pp. 625-636.
- Nakagaki, H., Kitagaki, K., Ogasawara, T. and Tsukune, H. (1997), "Study of deformation and insertion tasks of a flexible wire", *IEEE International Conference on Robotics and Automation (ICRA)*, Albuquerque, NM, pp. 2397-2402.
- Quinlan, S. (1994), "Real-time modification of collision-free paths", PhD thesis, Stanford University, Stanford.
- Rambow, M., Schauß, T., Buss, M. and Hirche, S. (2012), "Autonomous manipulation of deformable objects based on teleoperated demonstrations", *IEEE/RSJ International Conference on Intelligent Robots and Systems (IROS)*, Vilamoura, pp. 2809-2814.
- Ramirez-Alpizar, I.G., Harada, K. and Yoshida, E. (2014), "Motion planning for dual-arm assembly of ring-shaped elastic objects", *IEEE/RAS International Conference on Humanoid Robotics (Humanoids)*, Madrid, pp. 594-600.
- Saha, M. and Isto, P. (2007), "Manipulation planning for deformable linear objects", *IEEE Transactions on Robotics*, Vol. 23 No. 6, pp. 1141-1150.
- Sakamoto, N., Higashimori, M., Tsuji, T. and Kaneko, M. (2007), "An optimum design of robotic hand for handling a visco-elastic object based on Maxwell model", *IEEE International Conference on Robotics and Automation (ICRA)*, Rome, pp. 1219-1225.
- Shoushtari, A.L., Leylavi Shoushtari, A., Mazzoleni, S. and Dario, P. (2016), "Bio-inspired kinematical control of redundant robotic manipulators", *Assembly Automation*, Vol. 36 No. 2, pp. 200-215.
- Villareal, A. and Asada, H. (1991), "A geometric representation of distributed compliance for the assembly of flexible parts", *IEEE International Conference on Robotics and Automation (ICRA)*, Sacramento, CA, Vol. 3, pp. 2708-2715.
- Vinh, T.V., Tomizawa, T., Kudoh, S. and Suehiro, T. (2012), "A new strategy for making a knot with a general-purpose arm", *IEEE International Conference on Robotics and Automation (ICRA)*, Saint Paul, MN, pp. 2217-2222.
- Wakamatsu, H., Tsumaya, A., Arai, E. and Hirai, S. (2006), "Manipulation planning for unraveling linear objects", *IEEE International Conference on Robotics and Automation (ICRA)*, Orlando, FL, pp. 2485-2490.
- Wakamatsu, H., Hirai, S. and Iwata, K. (2004), "Static analysis of deformable object grasping based on bounded force closure", *IEEE/RSJ International Conference on Intelligent Robots and Systems (IROS)*, New Orleans, LA, Vol. 2, pp. 1719-1725.
- Wakamatsu, H., Tsumaya, A., Arai, E. and Hirai, S. (2004), "Planning of one-handed knotting/unraveling manipulation of linear objects", *IEEE International Conference on Robotics and Automation (ICRA)*, New Orleans, LA, Vol. 2, pp. 1719-1725.
- Wang, W., Bell, M.P. and Balkcom, D. (2015), "Towards arranging and tightening knots and unknots with fixtures", *IEEE Transactions on Automation Science and Engineering*, Vol. 12 No. 4, pp. 1318-1331.
- Wolter, J. and Kroll, E. (1996), "Toward assembly sequence planning with flexible parts", *IEEE International Conference on Robotics and Automation (ICRA)*, Minneapolis, MN, pp. 1517-1524.
- Yamakawa, Y., Namiki, A. and Ishikawa, M. (2010), "Motion planning for dynamic knotting of a flexible rope



- with a high-speed robot arm”, *IEEE/RSJ International Conference on Intelligent Robots and Systems (IROS)*, Taipei, pp. 49-54.
- Yamakawa, Y., Namiki, A. and Ishikawa, M. (2012), “Simple model and deformation control of a flexible rope using constant, high-speed motion of a robot arm”, *IEEE International Conference on Robotics and Automation (ICRA)*, Saint Paul, MN, pp. 2249-2254.
- Yoshida, E., Ayusawa, K., Ramirez-Alpizar, I.G., Harada, K., Duriez, C. and Kheddar, A. (2015), “Simulation-based optimal motion planning for deformable object”, *IEEE International Workshop on Advanced Robotics and its Social Impacts (ARSO)*, July, Lyon.
- Yue, S. and Henrich, D. (2002), “Manipulating deformable linear objects: sensor-based fast manipulation during

- vibration”, *IEEE International Conference on Robotics and Automation (ICRA)*, Washington, DC, pp. 2467-2472.
- Zheng, Y.F., Pei, R. and Chen, C. (1991), “Strategies for automatic assembly of deformable objects”, *IEEE International Conference on Robotics and Automation (ICRA)*, Sacramento, CA, Vol. 3, pp. 2598-2603.
- Zucker, M., Ratliff, N., Dragan, A.D., Pivtoraiko, M., Klingensmith, M., Dellin, C.M., Bagnell, J.A. and Srinivasa, S. (2013), “CHOMP: Covariant Hamiltonian optimization for motion planning”, *International Journal of Robotics Research (IJRR)*, Vol. 32 No. 9/10, pp. 1164-1193.

**Corresponding author**

**Ixchel G. Ramirez-Alpizar** can be contacted at: [ramirez@sys.es.osaka-u.ac.jp](mailto:ramirez@sys.es.osaka-u.ac.jp)